NASA Contractor Report 2911

Prediction of Compliant Wall Drag Reduction - Part I

Steven A. Orszag

CONTRACT NAS1-14275
NOVEMBER 1977

NASA

NASA Contractor Report 2911

Prediction of Compliant Wall Drag Reduction - Part I

Steven A. Orszag
Cambridge Hydrodynamics, Inc.
Cambridge, Massachusetts

Prepared for
Langley Research Center
under Contract NAS1-14275

National Aeronautics
and Space Administration

**Scientific and Technical
Information Office**

1977

TABLE OF CONTENTS

PREDICTION OF COMPLIANT WALL DRAG REDUCTION - PART I

Steven A. Orszag
Cambridge Hydrodynamics, Inc.
Cambridge, Massachusetts 02139

1. INTRODUCTION

This report discusses the formulation, development, and some applications of a numerical model of the effect of compliant walls on turbulent boundary layer flows. Since skin-friction drag accounts for about half the drag on long-haul aircraft, any reduction in this drag is of great importance in improving fuel economy and aircraft range as well as increasing payload efficiency and decreasing environmental pollution.

The current state of experimental and theoretical research on compliant walls and their effect on turbulent boundary layers has been reviewed by Fischer, Weinstein, Ash & Bushnell[1] and by Bushnell, Hefner & Ash[2]. A survey of various alternative techniques for aircraft drag reduction has been given recently by Hefner, Bushnell, Whitcomb, Cary & Ash[3] (Ref. 2 is reproduced as a chapter in Ref. 3). In summary, the current state of both experiments and theory is inconclusive. Some experiments show a substantial effect of compliant walls on drag, others do not. It is not clear that conventional materials can serve as suitable compliant boundaries to give drag reduction, though there

do seem to be some attractive possibilities. It is only clear that drag reduction by compliant walls is not as simple a phenomenon as may be suggested by cursory consideration of the hydrodynamical efficiency of dolphins.[4] Evidently, the dynamical characteristics of the wall are crucial in determining whether drag reduction or drag enhancement will result; the response of the wall must be matched in some dynamical sense still to be elucidated to the characteristics of the turbulent boundary layer over it. One of the principal purposes of the present work is to help in identifying the nature of the effect of the wall motions on the drag so that design of suitable walls can be expedited.

There have been several theoretical investigations of turbulent boundary layer flows over moving walls; a survey is given in Refs. 2,3. One of the most attractive ideas[2] for explaining drag reduction by compliant walls is that the wall influences the turbulent burst phenomenon by providing a pressure field that tends to inhibit bursts when they normally occur. This idea leads to significant qualitative understanding of the effect of compliant walls. In the present report, we discuss a numerical model based on the above idea and report quantitative tests of it as a mechanism of compliant wall drag reduction.

In Sec. 2, we discuss the proposed mechanism of compliant wall drag reduction. In Sec. 3, we discuss the numerical model of the mean flow motion. Then, in Sec. 4,

we discuss techniques for the investigation of the stability of the predicted mean flow profiles and for the prediction of burst frequency. In Sec. 5, we present results of the present model for turbulent boundary layer velocity profiles during the burst phenomenon and use these results to fix various parameters of the model by comparison with experimental results. Then, in Sec. 6, we present numerical results for the combined mean-flow and stability analysis of the turbulent boundary layer flow over a compliant wall. In this analysis, we use a crude burst predictor based on amplification factors. Finally, in Sec.7, we summarize the current state of research on the turbulence flow model investigated here.

2. A PROPOSED MECHANISM OF COMPLIANT WALL DRAG REDUCTION

In the last decade, there has accumulated a wealth of experimental evidence that the process of burst formation in turbulent boundary layer flows is not completely random, but rather can be correlated with a set of reasonably well-ordered dynamical events. Thus, a plausible coherent sequence of events for formation and regeneration of bursts is as follows[5-7]:

1. 'Old' bursts produce a large adverse pressure pulse that moves at a speed of roughly $0.8U_\infty$ and has an amplitude of roughly $3p'_{rms}$, where p'_{rms} is the rms wall pressure fluctuation intensity.[5]

2. This adverse gradient retards the flow near the wall and produces a low-speed streak.

3. A new burst is created when the low-speed streak creates highly inflectional velocity profiles in the wall region.

4. The favorable part of the large-scale pressure pulse due to previous bursts tends to assist the new burst in 'sweeping' out away from the wall. Most of the Reynolds stress and turbulence production occurs during the burst and sweep process, with relatively low turbulence activity between bursts.

5. The 'new' bursts set up conditions similar to that discussed in 1. above and the whole sequence of events is repeated.

Bushnell[2] has proposed that the above sequence of events can be used to formulate a quantitative flow model for the prediction of properties of turbulent boundary layers. The idea is to impose the experimentally measured pressure pulse due to 'old' bursts, to model the background turbulence between bursts using a crude turbulence model, and then to calculate the inflectional mean-velocity profiles produced by the pressure pulse using a two-dimensional Navier-Stokes equation computer code. Finally, the occurence of new bursts can be investigated in this flow model by calculating the growth of Tollmien-Schlicting waves and using an amplitude-growth criterion[8] to predict the onset of new bursts.

Bushnell's turbulent boundary layer model also suggests a mechanism for drag reduction by compliant walls. If the wavelength of the wall motions is small (at most the wavelength of the imposed pressure pulse), the wall motion can interrupt the feedback loop outlined above somewhere between steps 2. and 4. If the short wavelength wall motions can delay burst formation through the adverse part of the imposed pressure pulse then the favorable part of the imposed pressure pulse may inhibit bursting. In this case, turbulence production and turbulent boundary-layer drag are decreased.

The present work is motivated by the above ideas of Bushnell. The model seeks to determine quantitatively whether realistic wall motions and imposed pressure pulses interact in a time-dependent environment in such a way as to decrease burst frequency and wall drag. The present

work concentrates on the numerical study of the mean velocity profiles produced by the imposed pressure pulse. We use a relatively crude technique to investigate the stability of the resulting profiles (see Sec. 4). Only a limited number of different cases have been examined to date and the conclusions regarding the flow model are not yet certain. It seems that if the wavelength of the wall motions is large (of order the length of the imposed pressure pulse), there is no drag reduction. However, if the wavelength of the wall motions is very small (shorter than the sublayer thickness), substantial drag reduction may occur (although our computer runs at such short wavelengths may have just marginal accuracy). Future work must test the flow model further, particularly with respect to intermediate wavelength wall motions and more accurate flow stability calculations.

3. NUMERICAL MODEL FOR THE MEAN FLOW

In this Section, we discuss the numerical techniques used to solve the equations of Bushnell's turbulent boundary layer model discussed in Sec. 2. We solve the two-dimensional Navier-Stokes equations with a background turbulence model, inflow-outflow boundary conditions, and imposed large-scale pressure pulse at 'infinity'. The resulting mean-flow profiles show the effect of the pressure pulse in distorting (retarding) the mean profiles and in producing inflectional profiles.

The two-dimensional Navier-Stokes equations for incompressible flow are

$$\frac{\partial \vec{v}}{\partial t} + \vec{v}\cdot\vec{\nabla}\vec{v} = -\vec{\nabla}p + \vec{\nabla}\cdot\underset{\approx}{T} + \vec{f} \qquad (3.1)$$

$$\vec{\nabla}\cdot\vec{v} = 0 \qquad (3.2)$$

where $\vec{v}(x,y,t)$ is the two-dimensional velocity field, $p(x,y,t)$ is the pressure, $\underset{\approx}{T}$ is the stress tensor, and $\vec{f}$ is an imposed external force. We solve (3.1) in a channel: $0 \leq x \leq L$ and $0 \leq y \leq H$. In a typical run, the values of L and H are L = 600 and H = 200 in units non-dimensionalized by the length ν/U_τ where U_τ is the friction velocity and ν is the kinematic viscosity.

We approximate the stress tensor $\underset{\approx}{T}$ by retaining only its x-y component:

$$T_{xy} = -\overline{u'v'} + \nu\frac{\partial U}{\partial y}$$

where ν is the viscosity, U is the mean velocity, and u' and v' are the x and y components, respectively, of the

velocity fluctuations. The Reynolds stress, $-\overline{u'v'}$, is then evaluated by Van Driest's empirical formula[9] so that

$$\tau_{xy} = [B(.4y)^2 \left|\frac{\partial U}{\partial y}\right| (1 - e^{-A_y U_\tau/\nu})^2 + \nu] \frac{\partial U}{\partial y} \qquad (3.3)$$

where the constant A is chosen to be .04 in agreement with experimental measurements of turbulent boundary-layer mean-velocity profiles. The constant B is an ad hoc correction to the usual Van Driest formula that accounts for the fact that the turbulence level between bursts is small; a typical value for the background turbulence scale constant B in our calculations is B = .05.

Boundary conditions

The boundary conditions to be imposed on (3.1-2) require more detailed discussion. Each of the four boundaries x = 0, L, y = 0, H poses its own special kind of boundary condition problem. Let us begin by a brief analysis of boundary conditions for (3.1-2). We do this by an energy analysis that establishes a uniqueness theorem for the Navier-Stokes equations.

Consider two flows $\vec{v}_1(x,y,t)$ and $\vec{v}_2(x,y,t)$ that both satisfy the same boundary conditions and that both satisfy (3.1-2). In this case $\vec{v}(x,y,t) = \vec{v}_1(x,y,t) - \vec{v}_2(x,y,t)$ satisfies the equations

$$\frac{\partial \vec{v}}{\partial t} + \vec{v}_1 \cdot \vec{\nabla}\vec{v} + \vec{v} \cdot \vec{\nabla}\vec{v}_2 = -\vec{\nabla}p + \vec{\nabla} \cdot \underset{\approx}{T}$$

where $p = p_1 - p_2$ and $\underset{\approx}{T} = \underset{\approx}{T}_1 - \underset{\approx}{T}_2$. It follows that the perturbation energy E(t) defined by

$$E(t) = \tfrac{1}{2} \int_D v^2 \, dx$$

satisfies

$$\frac{dE}{dt} = -\frac{1}{2} \int_{\partial D} v^2 \vec{v}_1 \cdot \vec{n}_{out} \, d\Sigma - \int_{\partial D} p\vec{v} \cdot \vec{n}_{out} \, d\Sigma$$

$$- \int_D \vec{v} \cdot (\vec{v} \cdot \vec{\nabla}) \vec{v}_2 \, d\vec{x} + \int_D u \frac{\partial T_{xy}}{\partial y} \, d\vec{x}$$

where ∂D is the boundary of the computational domain D, $\vec{n}_{out}$ is the outward normal on ∂D, and $d\Sigma$ is the surface element on ∂D. It follows that if

$$M = \max_{\vec{x} \in D} |\vec{\nabla} \vec{v}_2|$$

and

(i) p is specified on all of D and $\vec{v} \cdot \vec{n}_{out}$ is specified on all of ∂D where $\vec{v} \cdot \vec{n}_{out} < 0$ and T is specified on all of D: or (ii) $\vec{v} \cdot \vec{n}_{out}$ is specified on all of D and $\vec{v}$ is specified at all points where $\vec{v} \cdot \vec{n}_{out} < 0$, then

$$\frac{dE}{dt} \leq 2M \, E(t)$$

Therefore, if either of conditions (i) or (ii) holds at each point of the boundary of the computational domain, the error energy E(t) grows at most exponentially with t, so the problem is well posed.

Using the above analysis, we can specify physically interesting boundary conditions for Bushnell's turbulent boundary layer model. We treat the four boundary surfaces individually.

<u>x = 0</u>

Here the flow is assumed to enter the computational

domain. Since the boundary is an inflow boundary, it is physically reasonable to assume that both components of the velocity field are known at x = 0. Thus, we impose the inflow boundary conditions that u(0,y,t) and v(0,y,t) are both known for all y and t.

x = H

This boundary is an outflow boundary. Since the only non-vanishing component of the Van Driest Reynolds stress tensor (3.3) is T_{xy}, it follows that the Navier-Stokes equations (3.1-2) are parabolized in the x direction. Therefore, according to (i), we need only impose boundary conditions on the outflow component of the velocity $\vec{v}\cdot\vec{n}_{out} = u(L,y,t)$.

However, imposition of boundary values on u(L,y,t) directly will give some difficulty because it will generate boundary layers near the outflow point x = L. Therefore, we impose the weaker boundary condition

$$u_{xx}(L,y,t) = 0 \qquad (3.4)$$

Boundary conditions like (3.4) are known to have small upstream influence so they do not disturb the main region of computation which is away from the downstream boundary x = L.

y = 0

This is the location of the compliant wall. If the wall were rigid, we would impose the boundary conditions

$$v(x,0,t) = 0 \qquad (3.5)$$

There are two effects of a moving boundary at $y = 0$. First, the boundary location is shifted to $y = \eta(x,t)$. Second, the wall motion as a function of t requires the velocity to be nonvanishing at the wall. The proper boundary condition at the wall is that there is no relative motion of the wall and the fluid at the wall-fluid interface.

We impose boundary conditions at the moving wall by assuming linearized wall motion. This assumption is a great simplification and is justified because the wall motions of interest are not large compared to the sublayer thickness. It follows that the vertical wall motion is

$$v = \frac{D\eta}{Dt} = \frac{\partial \eta}{\partial t} + U \frac{\partial \eta}{\partial x} \tag{3.6}$$

where $U = Dx/Dt$ is the component of wall motion in the direction tangent to the wall. Eq. (3.6) for the vertical wall motion v is true nonlinearly. Linearization of the wall motion implies that all quantities in (3.6) may be evaluated at the undisturbed wall location $y = 0$.

In order to complete the specification of boundary conditions at $y = 0$, it is necessary to know $U(x,t)$, the tangential component of the wall motion. This quantity depends on the physical model of the compliant wall, and must be specified in addition to the vertical wall motion $\eta(x,t)$. In the present work, we do not determine the wall motions self-consistently, in the sense that we impose $\eta(x,t)$ and do not determine the effects of wall pressure fluctuations due to the turbulent boundary flow on the motion of the wall.

Most of the materials of current interest for compliant wall drag reduction applications are flexible materials that can 'stretch' in the y-direction but have little lateral freedom for movement in the x-direction. Therefore, because of the lack of specific information on this point, we have chosen the wall boundary condition $U(x,t) = 0$. Admittedly, this is oversimplified, but a detailed model of the wall is necessary before this boundary condition can be improved.

It is not generally recognized that both $\eta(x,t)$ and $U(x,t)$ must be specified to determine the wall motion. However, consider the simple wall motion $y = \eta(t)$, independent of x. The motion of the wall in its plane $y = \eta(t)$ can be arbitrary and the proper tangential boundary conditions are

$$u(x,\eta,t) = U(x,t)$$

$\underline{y = H}$

The boundary conditions imposed at the top of the layer $y = H$ are the most unusual, and the most difficult to get right (see below). In order to model the large-scale pressure pulse due to old bursts, we want to impose the value of the pressure $p(x,H,t)$ at the top of the layer. According to our analysis of boundary conditions, this obviates the need to impose the vertical (normal) component of velocity $v(x,H,t)$ at an outflow point.

However, on physical grounds we expect the magnitude of the normal velocity at the top of the layer to have profound effects on our ability to model the bursting

process. In fact, we have found by numerical experimentation with Bushnell's model (see Sec. 5) that there is extreme sensitivity of the model to the normal component of velocity at y = H. Therefore, we have assumed as a crude model of this effect that there is uniform inflow at all points of the boundary y = H of magnitude -V:

$$v(x,H,t) = -V \tag{3.7}$$

where V is non-negative. Since the boundary y =H is now an inflow boundary, it seems to be also necessary to specify u(x,H,t). However, it is not difficult to show that this would overspecify the boundary conditions at y = H because u(0,y,t) is specified.

In computations with rigid walls, the imposition of the boundary conditions that p(x,H,t) and v(x,H,t) are specified has seemed to be satisfactory, except for some slight difficulty near the intersection of the outflow boundary x = H and the lid y =L; this difficulty due to a very thin outflow boundary layer was circumvented by introducing additional dissipation locally near x = L, y = H in the numerical computations. However, in some recent computations with compliant walls with wavelengths intermediate between the sublayer thickness and the pressure pulse wavelength, we have encountered numerical instability that appears to be due to the top boundary conditions. This difficulty is still under active investigation, but it should not affect in any way the results presented in Sects. 5-6.

Numerical methods

We solve (3.1-2) with the boundary conditions discussed above using a mixed spectral-finite difference method. The vertical (y) direction is resolved using expansions in Chebyshev polynomials, while the x-direction is resolved using a second-order staggered-grid finite difference scheme. Thus, we represent the velocity field by

$$\vec{v}(j\Delta x,y,t) = \sum_{n=0}^{N} \vec{u}_n(j\Delta x,t)T_n(2y/H-1) \qquad (3.8)$$

where Δx is the grid separation in x and $T_n(y)$ is the Chebyshev polynomial of degree n, defined by

$$T_n(\cos\theta) = \cos n\theta \ .$$

A review of spectral methods and finite-difference methods used here as been given elsewhere.[11,12] Let us just summarize here some of the important properties of these methods:

i) The use of Chebyshev polynomials in y is infinite-order accurate, in the sense that errors go to zero faster than any finite power of 1/N as $N \to \infty$.

ii) The use of Chebsyhev polynomials in y yields efficient calculations if use is made of fast Fourier transforms.

iii) Chebyshev polynomials allow accurate resolution of boundary layers; typically, if there are boundary layers of thickness ε , they can be resolved using only $1/\sqrt{\varepsilon}$ polynomials.

iv) The use of a staggered grid in the x-direction gives results roughly equivalent to those achieved by non-staggered grids with twice the spatial resolution.

v) The solution of the Poisson equation for the pressure field p is accomplished by fast Fourier transform in x and then reduction of the equations for the y-Chebsyhev coefficients to a tridiagonal system of equations. The resulting tridiagonal system can be solved efficiently using the LU-factorization algorithm in only order N operations. After Fourier transformation in x, the Poisson equation for the pressure takes the form of the system of uncoupled two-point boundary value problems

$$\frac{d^2p}{dy^2} - k^2 p = f(k,y) \tag{3.9}$$

When p is expanded in a Chebyshev series in y, the resulting equations for the Chebyshev coefficients $p_n(k)$ in the expansion

$$p(k,y) = \sum_{n=0}^{N} p_n(k) T_n(y) \tag{3.10}$$

are given in the tau approximation by[12]

$$-\frac{p_{n-2}}{4n(n-2)} + \left(\frac{1}{k^2} + \frac{1}{2n^2-2}\right) p_n - \frac{p_{n+2}}{4n(n+1)} = \mathcal{L} f_n(k) \tag{3.11}$$

The boundary conditions become

$$\begin{aligned} \Sigma(-1)^n n^2 p_n &= A \\ \Sigma p_n &= B \end{aligned} \tag{3.12}$$

The tridiagonal system (3.11-12) is essentially diagonally dominant so that LU-decomposition is numerically well conditioned.

vi) We use Adams-Bashforth time differencing of the nonlinear terms, together with a semi-implicit time-differencing scheme for the diffusive terms of the Van Driest Reynolds stress and for the inflow terms at $y = 0$ and $y = H$. Because the Chebyshev-polynomial expansions have so much resolution at the top and the bottom of the channel, they would give extremely stringent time-step retrictions on the Adams-Bashforth scheme. We avoid this difficulty by a semi-implicit method in which the terms that would cause the time-step retrictions to be severe are treated implicitly, thereby avoiding the time step restrictions. Details of this process are given in Refs. 12-13.

For the present problem, the terms that give unreasonable time-step restrictions are just the diffusive term and the terms representing advection through the top and bottom boundaries. These terms are easily treated semi-implicitly by subtracting from both sides of (3.1) constant coefficient diffusive and convective terms that bound the troublesome terms.[12] These subtracted terms are easily treated implicitly because they are constant coefficient terms.

vii) The code is also formulated in such a way that a moving coordinate system in x can be used as an option. This option is not used, however, in the calculations reported in Sects. 5-6.

4. NUMERICAL METHODS FOR STABILITY CALCULATIONS

Once the mean-flow profiles are calculated by the computer code described in Sec.3, we study the stability of the resulting flow by solution of the Orr-Sommerfeld equation for temporally growing disturbances in steady, plane-parallel two-dimensional incompressible flow. There are three important approximations made in this study which should be elminated in further work on this problem. First, we calculate only temporally growing disturbances, so we must convert between temporal growth and spatial growth using a group velocity transformation.[14] In our preliminary calculations of the stability of the mean-flow profiles we have been even cruder; instead of using the group-velocity transformation, we have transformed using the more readily calculated phase velocity $v_{ph} = \omega/k$, where ω is the frequency of the disturbance and k is its wavenumber in the x-direction. For the kinds of distrubances under present study, the approximation of the group velocity by the phase velocity should not introduce errors larger than 20%.

Second, by assuming the mean-flow to be steady we neglect possibly very important phase-coherence effects which could strongly affect growth rates. We have included time-variation of the mean flows only through the effect of using different profiles at different times in the evolution of a wave packet. The justification for the approximation of steady flow is weak; a non-steady flow stability analysis requires calculation of the eigenvalues of a Floquet theory and is best done for the present problem by solution of the full linearized Navier-

Stokes equations.

The third limitation of the present kind of stability analysis is the assumption that the flow is plane-parallel in x. In fact, the mean-flow profiles we determine by the computer code described in Sec. 3 are space varying. Part of the effect of the space variation is accounted for by use of different profiles in the study of stability of a wave-packet. However, the best way to study stability of a time-varying, space-varying flow of the sort encountered in the Bushnell turbulent boundary layer model is to solve the linearized Navier-Stokes equations in the channel $0 \leq x \leq L$, $0 \leq y \leq H$.. This task will be postponed to future work on the problem.

The Orr-Sommerfeld equation for the streamfunction of a linearized two-dimensional disturbance of the mean-flow profile $\bar{u}(y)$ is

$$\left(\frac{d^2}{dy^2} - \alpha^2\right)^2 v(y) = iR\left[(\alpha\bar{u}-\omega)\left(\frac{d^2}{dy^2} - \alpha^2\right) v - \alpha\bar{u}''v\right] \qquad (4.1)$$

with boundary conditions

$$v = v' = 0 \quad \text{at} \quad y = 0,H \qquad (4.2)$$

Here the streamfunction is assumed to have the form

$$v(y)e^{i(\alpha x-\omega t)} ,$$

where α is the wavenumber in the x-direction and ω is the (complex) frequency.

The Orr-Sommerfeld equation (4.1) with (4.2) is solved by expanding the eigenfunction $v(y)$ in a series of Chebyshev polynomials and then determining the eigenvalue ω by means of a matrix eigenvalue computer program based on the QR algorithm.[15] This procedure is very efficient and accurate.

We use the linear stability analysis outlines above to predict the occurrence of a burst as follows. First, we calculate the stability characteristics of various profiles at a fixed x location and various values of the time t. These calculations proceed until a time t_0 is found at which the profile is unstable ($\text{Im}\,\omega > 0$ for some wavenumber α). From that time onwards, we calculate the amplification ratio by the formula

$$\frac{A}{A_0} = \exp \int \text{Im}\,\omega \; dx/c \tag{4.3}$$

where we use the phase velocity $\text{Re}\,\omega/\alpha$ as an estimate of c (see above). The profiles whose stability is calculated are related in space-time by the relation

$$\Delta x = c\Delta t \tag{4.4}$$

Next, the Michel-Smith criterion[8] for occurrence of a burst is applied; a burst is presumed to occur if

$$\frac{A}{A_0} \approx e^9 \tag{4.5}$$

This empirical correlation has worked well for a variety of transition flows, but it is admittedly very crude and the power e^9 may be adjusted later after we get more experience with the present codes.

There are a number of refinements of the present stability calculations that should also be performed in the future. First, the linearized Navier-Stokes equations should be solved to account for nonparallel and nonsteady flow effects. Then, it may be useful to estimate the magnitude of nonlinear effects and to use a more realistic burst criterion than (4.5).

Some modifications in our present codes are possible that are significantly simpler than the linearized Navier-Stokes calculation mentioned above. First, the group velocity of the waves should be used instead of the phase velocity. Second, a spatial stability calculation should be performed instead of the present tmeporal stability calculations. Third, the effect of the inflow velocity -V imposed at y =H (see Sec. 3) should be included in the Orr-Sommerfeld equation; in fact, we have written our stability code to account for this latter effect, but it is not included in the calculations reported in Sec. 6.

5. FLAT PLATE RESULTS

In this Section, we report a number of numerical experiments performed to tune the Bushnell turbulent boundary layer model for flow over a flat plate. First, in Fig. 1, we show the results of a numerical experiment performed to test the accuracy of the Van Driest Reynolds stress (3.3) with B= 1 (full strength) in reproducing a turbulent boundary layer mean-velocity profile. The calculation (as well as the other calculations reported in this Section) used 33 Chebyshev polynomials to resolve the boundary layer (y) direction and 257 staggered grid points to resolve the downstream (x) direction. For the experiment (Run 1) plotted in Fig. 1, we impose the boundary conditions $p = v = 0$ at $y_+ = H = 200$. It is apparent from Fig. 1, that a turbulent boundary layer profile is well preserved in evolution from the upstream boundary at $x = 0$ to $x_+ = 200$ (and even beyond). This calculation shows that the upstream influence effect of the downstream boundary at $x_+ = 600$ is minimal -- in fact, no appreciable upstream influence of the boundary at $x_+ = 600$ is discernible beyond $x_+ = 500$.

The next set of runs we performed were designed to adjust the background turbulence level constant B in (3.3) and the inflow velocity v at $y_+ = H$, as well as to test the form of the required pressure pulse to achieve reasonable mean velocity profiles. The goal of these experiments

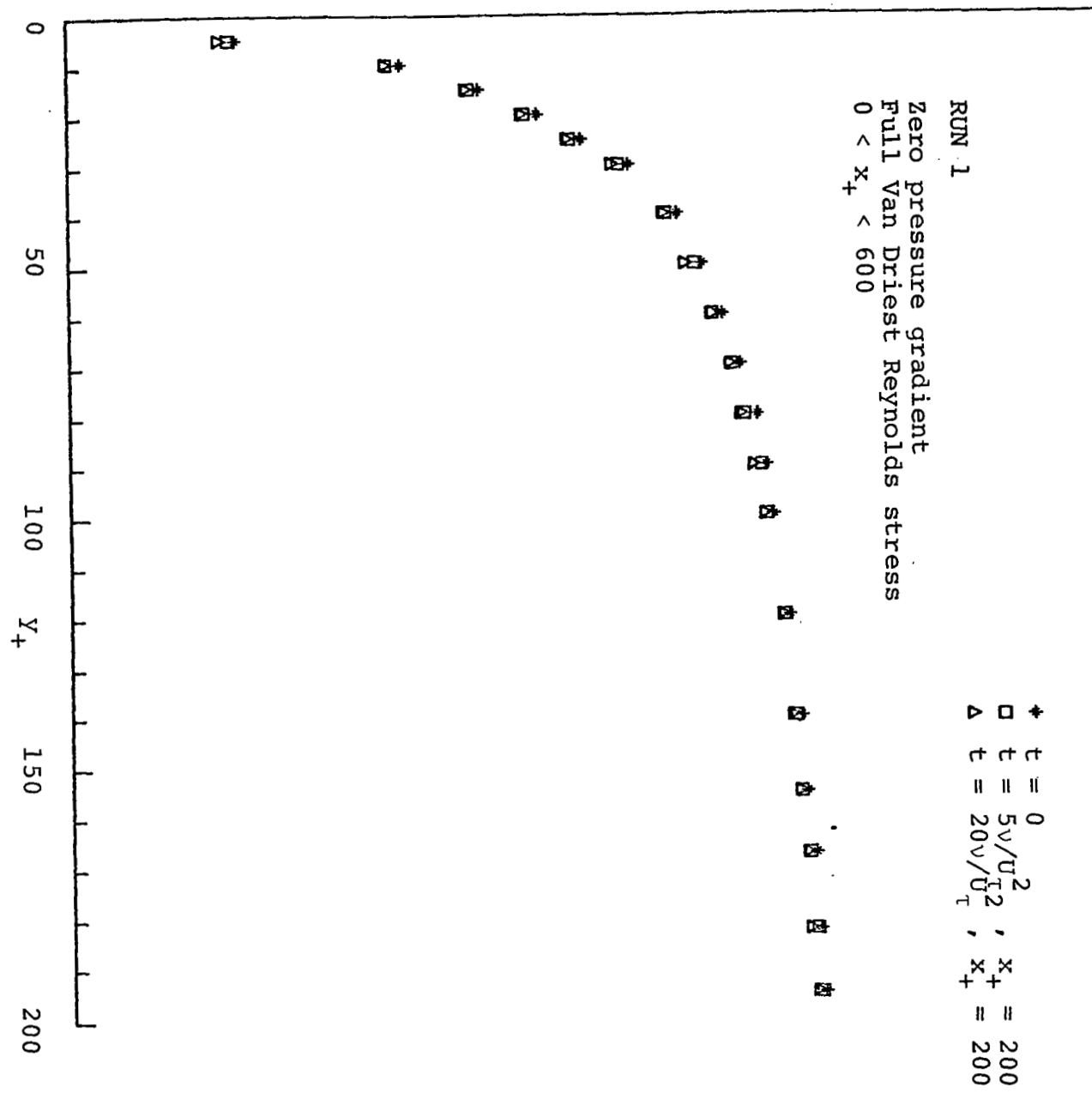

Figure 1. A plot of the calculated mean-velocity profiles for Run 1.

is to match the development of turbulent boundary layer profiles between bursts as measured by Blackwelder.[16] Some of Blackwelder's data for conditionally averaged velocity profiles before, during and after the period of burst formation are shown in Fig. 2. Observe the very strong inflectional profile at a time delay of -3.1 ms. This profile is strongly unstable and gives rise to a burst a short time later.

In Fig. 3, we plot the form of the pressure pulse used in our calculations of the Bushnell model. The magnitude of the pulse is chosen to be $3p'_{rms}$, in agreement with Burton's data[5] and to occur over a time period of 25 (in units of ν/U_τ^2 . The triangular form of this pulse is an arbitrary choice, but it is not too inconsistent with available experimental data. In some of the numerical experiments reported below, the amplitude of the pressure pulse is $2.5p'_{rms}$ and in some others the length of the pulse is decreased to 20.

In Fig. 4, we plot the results of a numerical calculation using the code described in Sec. 3 with $B = 0.05$ and $v = 0$ at $y_+ = H$, together with the imposed pressure pulse. The agreement with the Blackwelder profiles shown in Fig. 2 is not very good.

In Fig. 5, we plot the results of a similar experiment in which the vertical dimensionsion is truncated to $0 \leq y_+ \leq 100$, with the pressure pulse applied at $y_+ = 100$. The agreement with Blackwelder's measurements is even worse. We conclude from this comparison that the pressure pulse must be imposed in

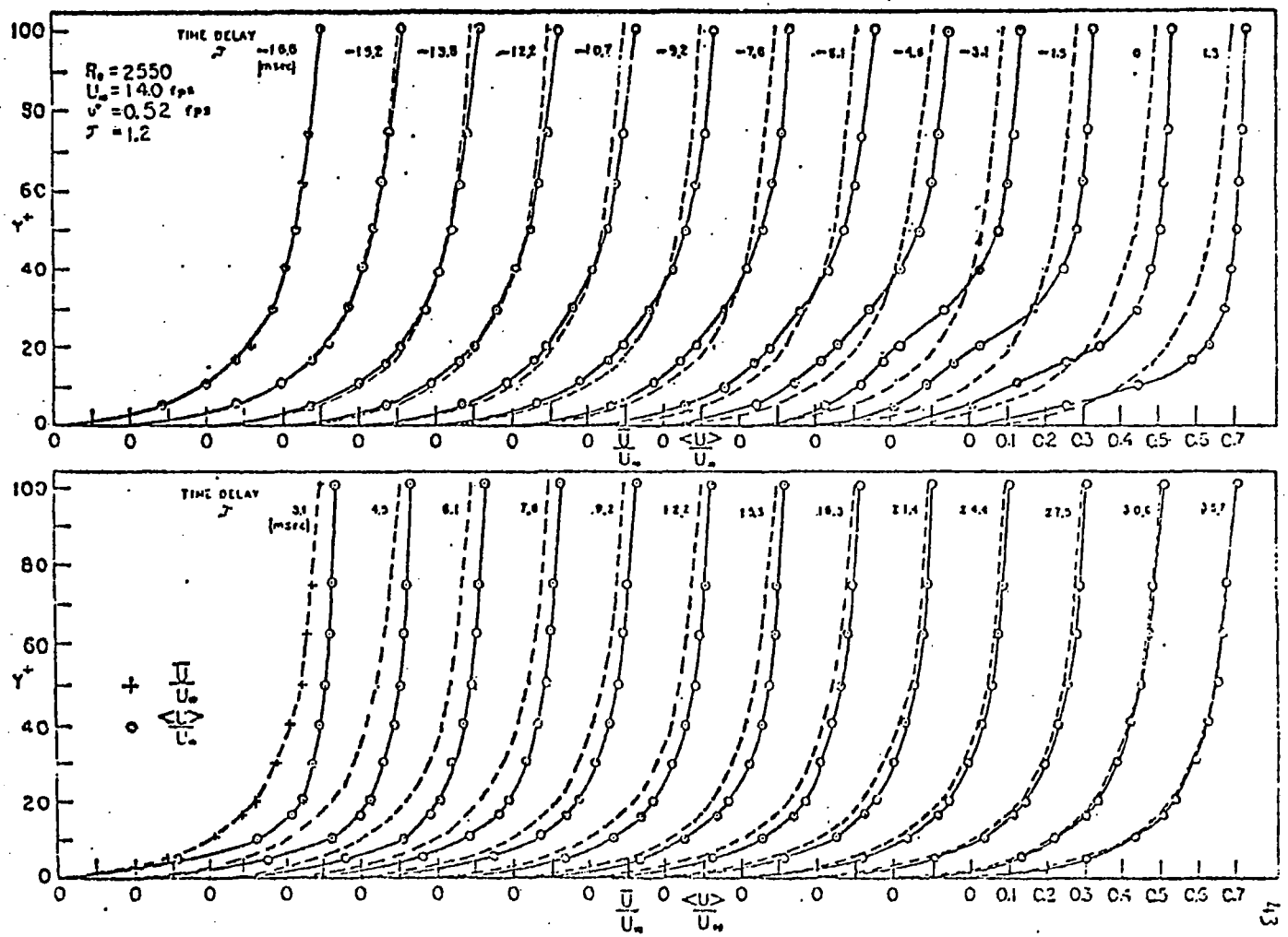

Fig. 2 - Conditionally averaged and mean velocity profiles with positive and negative time delay from the point of detection, (From Ref. 16).

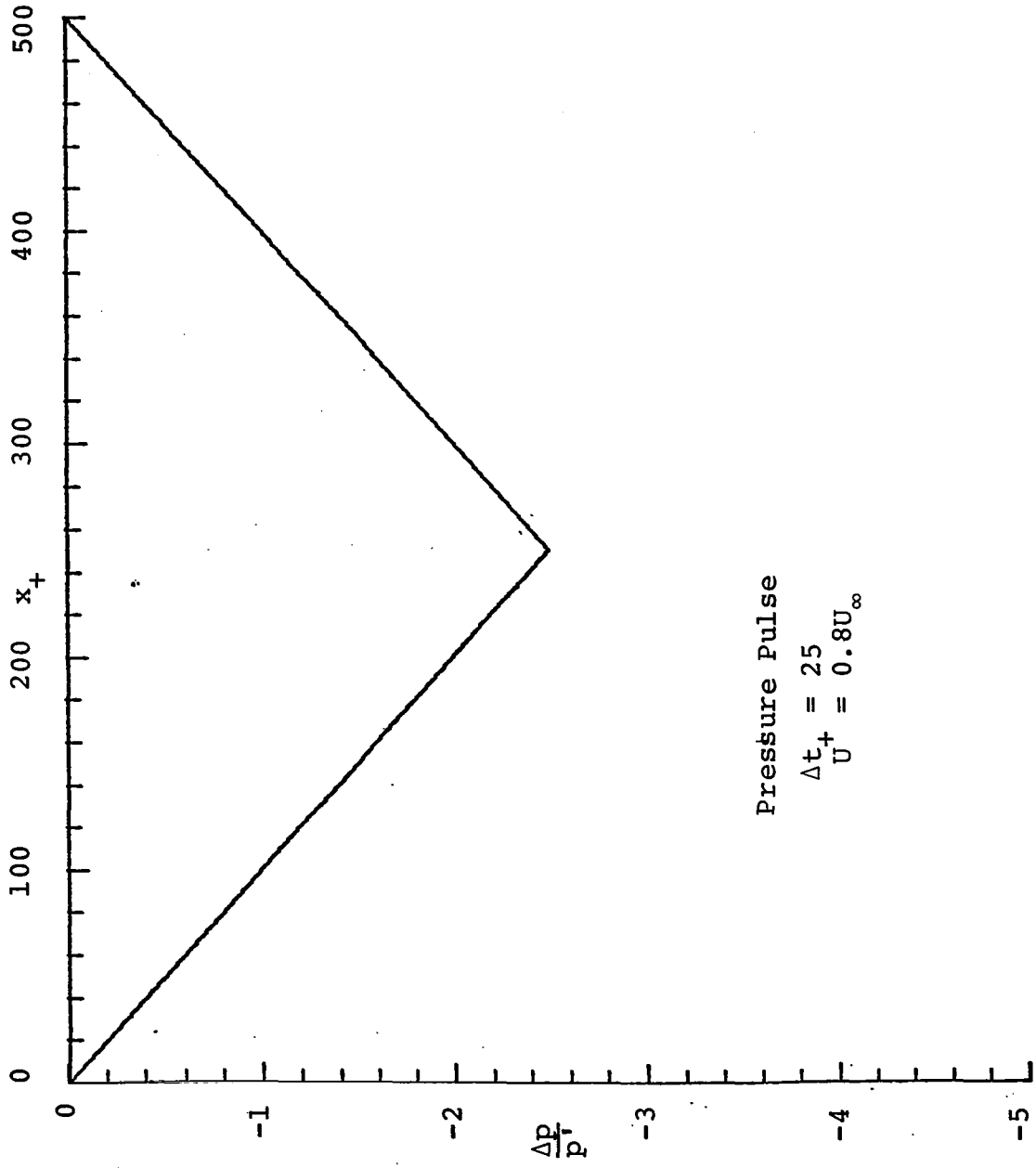

Figure 3. A plot of the imposed pressure pulse at $y_+ = H$. The form of this pulse is in good agreement with that measured by Burton.[5]

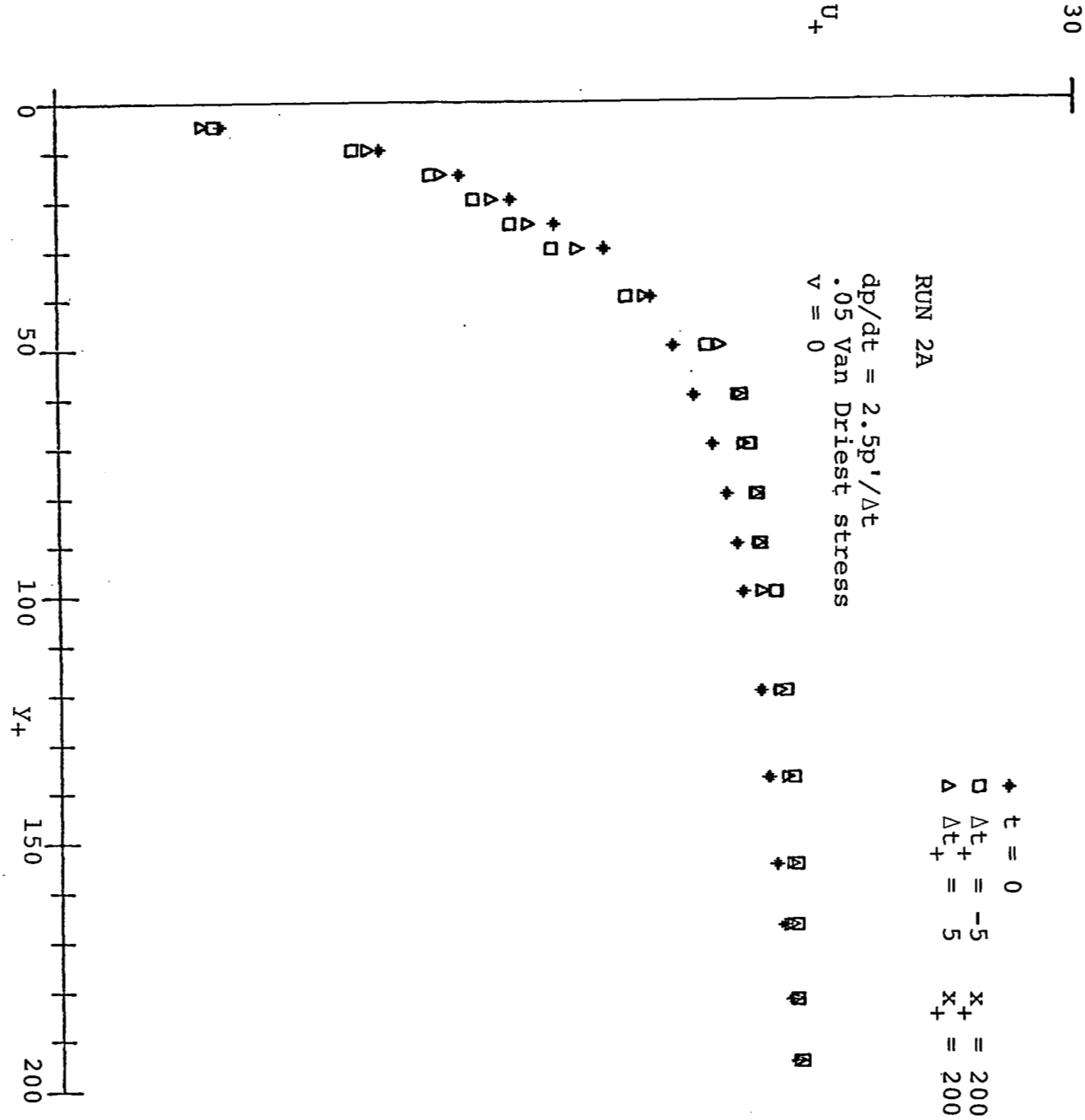

Figure 4. A plot of the calculated velocity profiles for Bushnell's model of the turbulent boundary layer. Time differences are measured from passage of the peak of the adverse pressure gradient pulse. The boundary conditions at the top of the layer are v = 0.

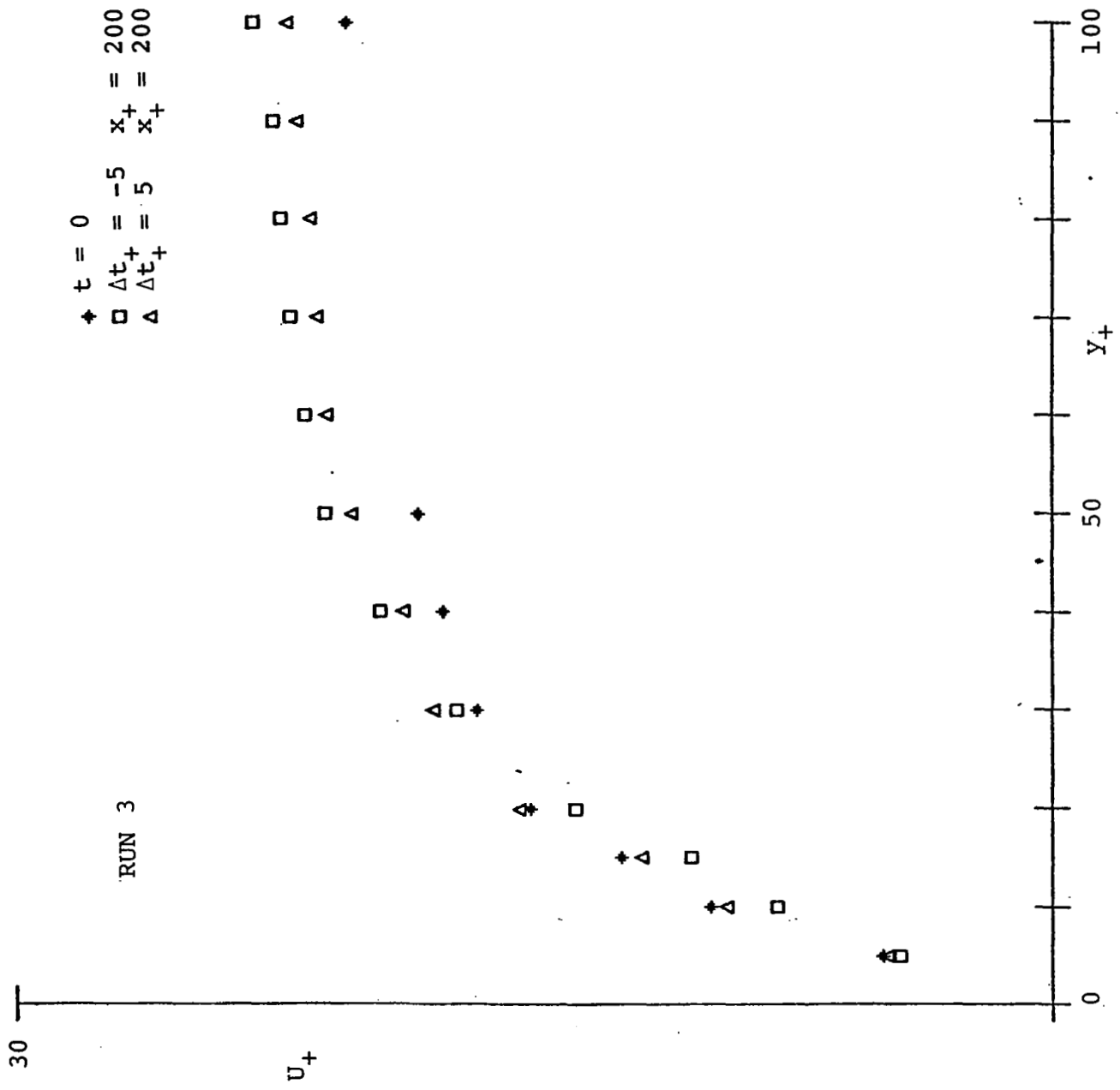

Figure 5. Same as Figure 4, except that the pressure pulse is applied at $y_+ = 100$ instead of $y_+ = 200$

the region y_+ 200, and certainly not so close to the wall as $y_+ = 100$.

In Fig. 6, we plot the results of a calculation similar to that shown in Fig. 4, except that the imposed inflow velocity at the top of the layer is $v = -0.5U$. In this case, the retardation due to the imposed pressure pulse is much larger than that shown in Fig. 4 and is in qualitative agreement with Blackwelder's results. Then, in Fig. 7, we plot the results of a calculation similar to the calculations plotted in Figs. 4 and 6, except that the inflow velocity at the top of the layer is $v = -2U$. In this case, the inflectional profile is very strong and even our two-dimensional mean-flow code with background turbulence model went unstable near the peak of the adverse pressure gradient pulse. This difficulty with Run 5 (shown in Fig. 7) is, we believe, unrelated to some calculational difficulties with intermediate wavelength compliant wall calculations reported later. We believe that the breakdown of Run 5 is due to the small value of $B = 0.05$, so that the background turbulence cannot stabilize (by diffusion) the unstable profile produced by the pressure pulse.

The conclusion to be drawn from Figs. 4-7 is that the strength of the inflectional profiles produced by passage of the pressure pulse is a very strong function of the inflow velocity v at the top of the boundary layer. It seems that $v \approx -0.5U$ gives results in reasonable quantitative agreement with Blackwelder's measurements.

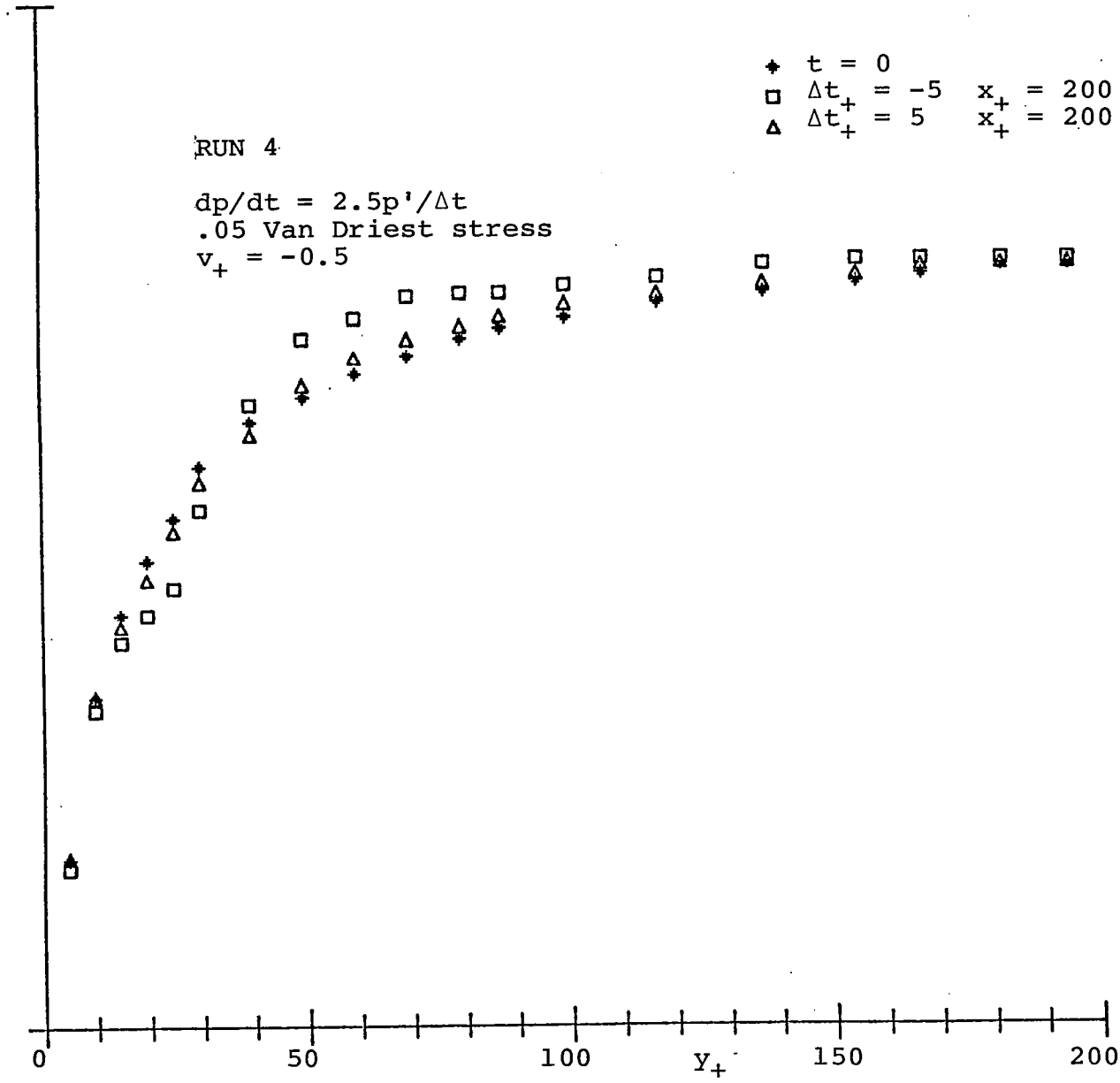

Figure 6. Same as Figure 4, except that an inflow velocity = -.5U is imposed at the top of the calculational domain, y_+=200.

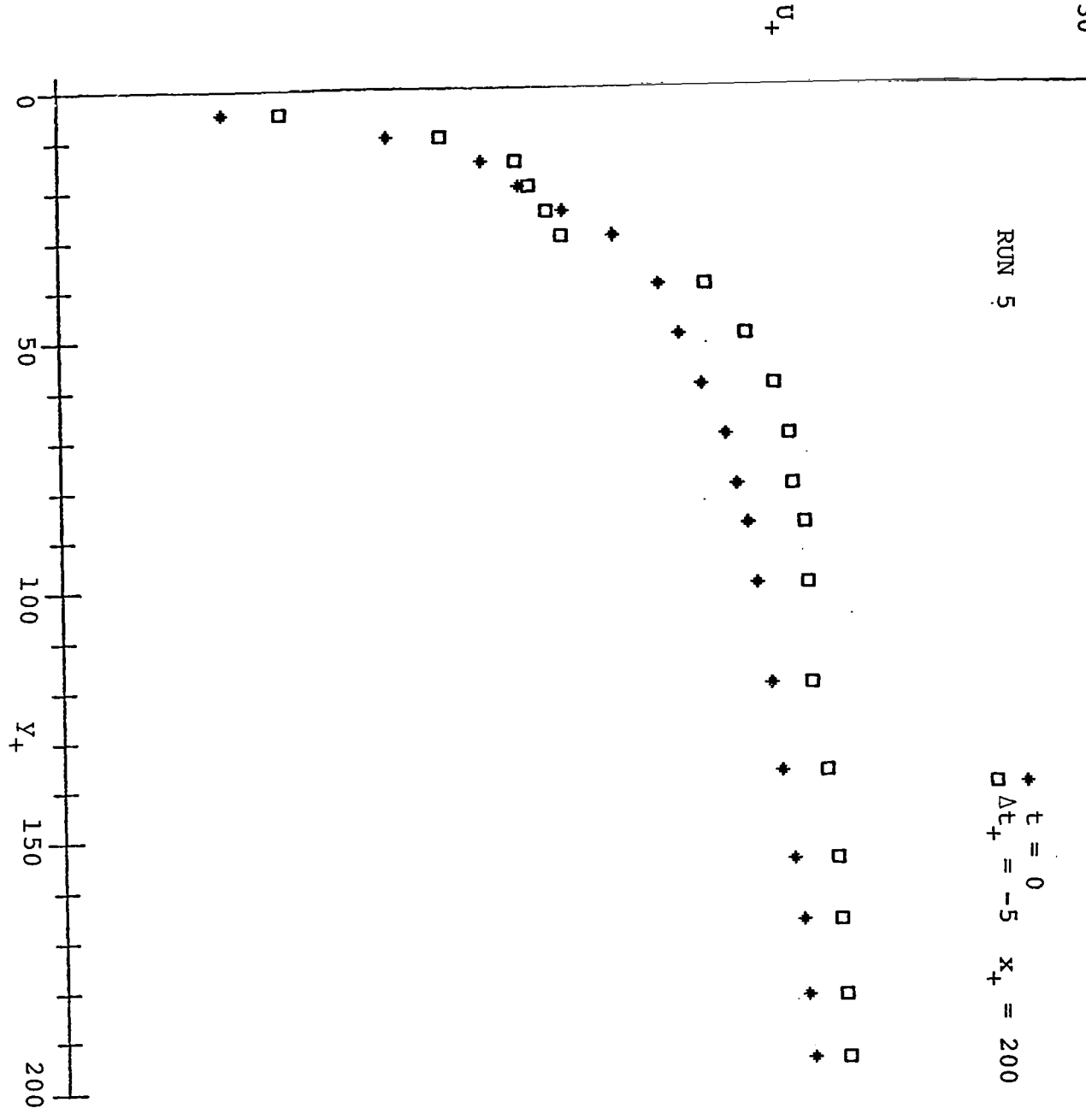

Figure 7. Same as Figure 4, except that an inflow velocity v = -2U is imposed at the top of the calculational domain.

6. COMPLIANT WALL RESULTS

We have performed several runs for the calculation of mean velocity profiles of a turbulent boundary layer over a compliant boundary with imposed wall motion. In all the experiments to date, we have assumed that the component of the wall motion in the direction of the mean flow vanishes: $U(x,t) = 0$. As discussed in Sec.3, the justification for this approximation is that typical compliant boundaries have supports that stiffen the medium to lateral deformation. Our computer code has run satisfactorily on cases in which the wavelength of the wall motion was both very long and very short. For example, in Fig. 8, we plot the results of a numerical calculation for a flow over a compliant boundary whose surface motion was a short wave,

$$\eta_+ = 5 \sin(2x_+ - 30\, t_+)$$

This wavelength is as short as can be resolved on our grid with 257 grid points in x.

We have also performed stability calculations for these flows over compliant moving walls. The amplification ratio A/A_0 is calculated as in Sec. 4 and the Michel-Smith correlation is used to predict the occurrence of a burst. In Fig. 9, we plot the amplification ratio vs time for a wavepacket originating at $x_+ = 200$ for Runs 4 (Fig. 6) and 7(Fig.8), in order to demonstrate the effect of a compliant wall. In Fig. 9, we plot the data two ways: the squares and triangles indicate the amplification factors obtained

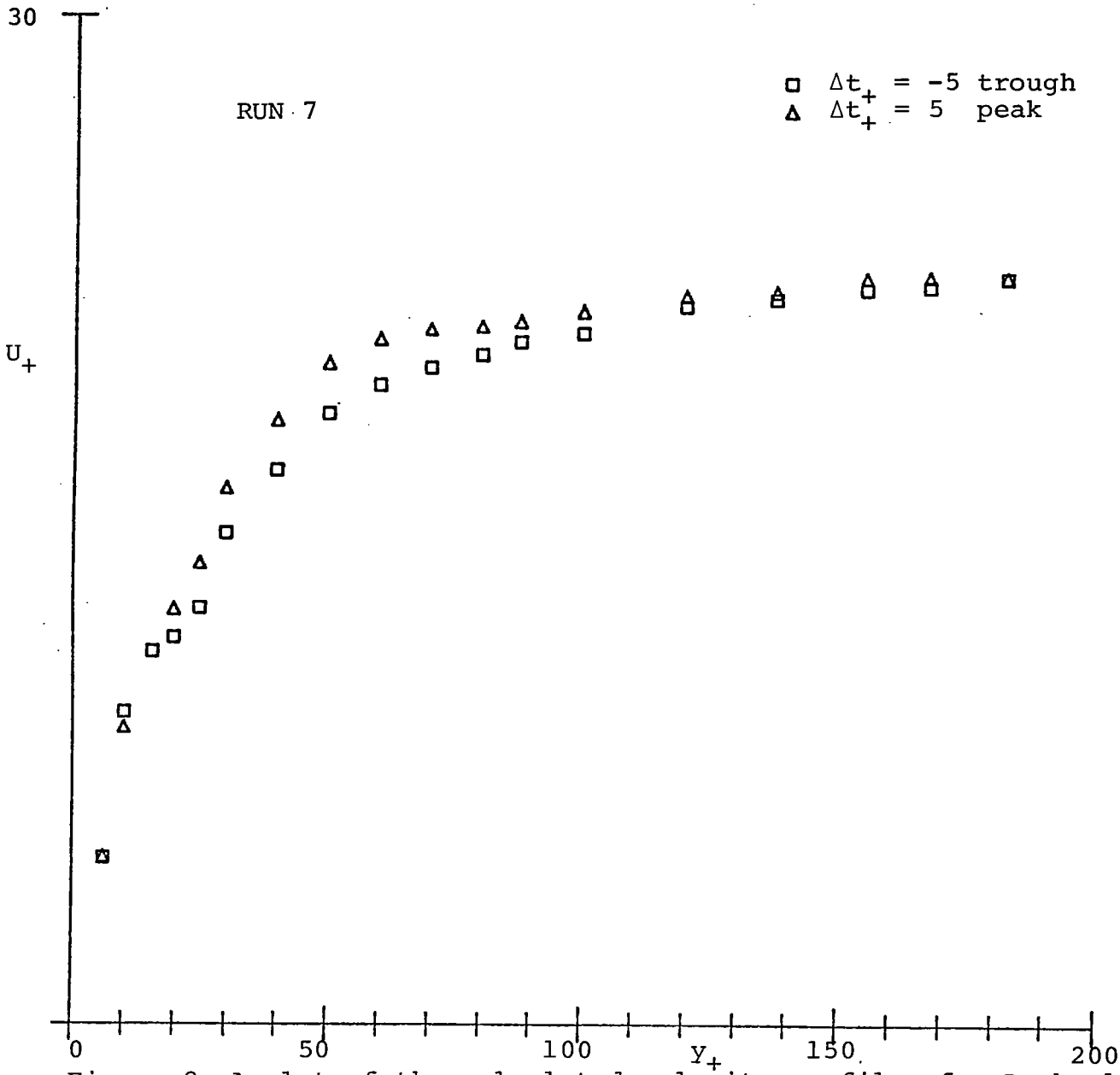

Figure 8. A plot of the calculated velocity profiles for Bushnell's model of the turbulent boundary layer over a moving wall. The imposed wall motion is a travelling sinusoid of amplitude $\eta_+ = 5$ and wavelength $\lambda_+ = \pi$ (short compared with the sublayer thickness).

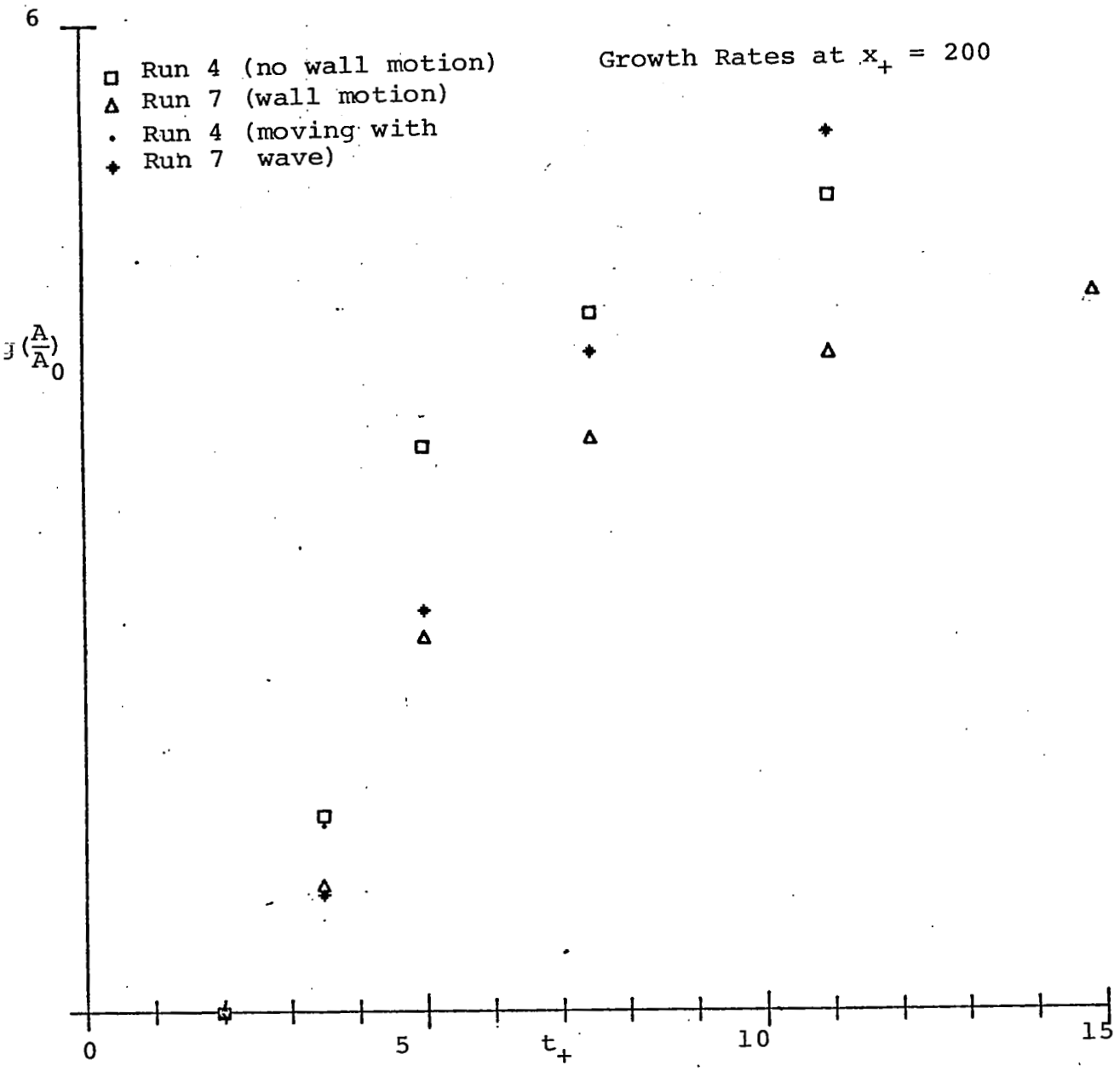

Figure 9. A plot of the amplification ratios of the most unstable disturbancesof the boundary layer profiles of Runs 4 and 7, which are identical except that Run 7 has a short wavelength imposed wall motion. Results are presented for disturbances following the wavepacket and for disturbances fixed at $x_+ = 200$.

by local stability analysis following the most unstable wave using a phase velocity transformation; the crosses and circles indicate the amplification factors obtained at a fixed location $x_+ = 200$, not following the wave.

The effect of the wall motion in decreasing the growth rate of disturbances in the boundary layer is apparent from the results plotted in Fig. 9 both following the wave and fixed in space. Also, the growth rates obtained following the wave are larger than those obtained fixed in space, apparently because when the packet moves it stays in a region of large amplification rate for a longer time and does not quickly encounter the favorable gradient portion of the pressure pulse.

Similar calculations for a long wavelength wall motion (wavelength = length of pressure pulse) indicate no drag reduction (and might indicate drag enhancement).

Unfortunately, the wavelengths indicated in Run 7 are probably much too small to be achieved by any practical compliant wall. Since long wavelengths seem to be de-stabilizing on the boundary layer while short wavelengths seem to be stabilizing, it seems that the goal of compliant wall drag reduction should be achieveable provided that dynamically light materials with short wavelength response can be found.

In order to quantify the longest wavelengths that seem to permit drag reduction, we began a series of numerical experiments with the code described in Sec. 3 with imposed wavelengths of order $x_+ = 100$. Unfortunately, we found a difficult numerical instability in the mean flow code so

no reliable results could be obtained. The instability does not seem to be similar to that of Run 5 at large times where the profiles become unstable due to large inflection. The instability in the present cases occur too early for this and seem to be related to an interaction between the imposed large-scale pressure pulse and the wall motion, perhaps reflecting an improperly posed mathematical problem where both p and the inflow velocity are specified as boundary conditions at the top of the layer. This problem is under active investigation and we hope to resolve it soon.

Since no evidence of any numerical instability is found in any of the results plotted in Figs. 1-9, we find no evidence that these results should be in error. However, it is apparent that an extensive series of numerical experiments should be performed to verify these results.

7. SUMMARY AND CONCLUSIONS

We have developed a set of computer codes to test Bushnell's boundary layer model. One code computes the evolution of mean velocity profiles during the period between bursts as forced by an imposed large-scale pressure pulse due to earlier bursts. Another code computes the local stability characteristics of these computed profiles. The programs use Chebyshev polynomials to resolve the boundary layer (y) direction and a staggered grid of mesh points to resolve the x direction. Typically, 257 grid points and 33 Chebyshev polynomials are used in the computations.

By carefully choosing the shape of the imposed pressure pulse, the level of background turbulence, the height of the computational region, and especially the inflow velocity at the top of the boundary layer, we are able to achieve reasonable agreement with Blackwelder's measured velocity profiles during the burst process on a flat plate.

Stability calculations of the resulting mean velocity profiles show that compliant moving walls with short wavelengths can have an appreciable effect in stabilizing the boundary layer to further bursts. On the other hand, long wavelength wall motions do not seem to limit the bursting process and, therefore, probably do not give significant drag reduction.

We are currently engaged in trying to obtain results concerning intermediate wavelength wall motions. However, an instability apparently due to the boundary conditions imposed at the top of the layer has prevented us from obtaining results

for these cases.

Future studies of Bushnell's boundary layer model should address the following problems:

(i) intermediate wavelength wall motions;

(ii) more accurate stability calculations using a linearized solution of the Navier-Stokes equations;

(iii)investigation of the effects of different kinds of wall motions, including possible motion of the wall in its own plane;

(iv) a complete investigation of different kinds of boundary conditions on the mean flow model and more extensive tests of the background turbulence model.

REFERENCES

1. M.C. Fischer, L.M. Weinstein, R.L.Ash, and D.M. Bushnell, "Compliant Wall-Turbulent Skin-Friction Reduction Research." AIAA Paper No. 75-833(1975).

2. D.M. Bushnell, J.N. Hefner, and R.L. Ash, "Compliant Wall Drag Reduction for Turbulent Boundary Layers." Phys. Fluids, to appear(1977).

3. J.N. Hefner, D.M. Bushnell, R.T. Whitcomb, A.M. Cary, Jr., and R.L. Ash, "Concepts for Drag Reduction." AGARD, R-654, June 1977, c.1977.

4. M.O. Kramer, " Hydrodynamics of the Dolphin." Adv. in Hydroscience 2, 111 (1965).

5. T.E. Burton, "The Connection Between Intermittent Turbulent Activity Near the Wall of a Turbulent Boundary Layer with Pressure Fluctuations at the Wall." Sc.D. Thesis, M.I.T. (Cambridge, Mass., 1974).

6. J. Laufer,"New Trends in Experimental Turbulence Research." Ann. Rev. Fluid Mech. 7, 307(1975).

7. W.W. Willmarth, "Structure of Turbulence in Boundary Layers." Adv. in Appl. Mech. 15(1975).

8. N.A. Jaffe, T.T. Okamura, and A.M.O. Smith, "Determination of Spatial Amplification Factors and Their Application to Predicting Transition." AIAA Journal 8, 301(1970).

9. E.R. Van Driest, "On Turbulent Flow Near a Wall." J. Aero. Sci. 23, 1007(1956).

10. P.J. Roache, Computational Fluid Dynamics, Hermosa Publ.(1972).

11. S.A. Orszag and M. Israeli, "Numerical Simulation of Viscous Incompressible Flows." Ann. Rev. Fluid Mech. 6, 281(1974).

12. D. Gottlieb and S.A. Orszag, Numerical Analysis of Spectral Methods, SIAM(1977).

13. S.A. Orszag,"Fourier Series on Spheres." Mon Weath. Rev. 102, 56(1974).

14. A. Michalke, "On Spatially Growing Disturbances in an Inviscid Layer." J. Fluid Mech. 23, 521(1965).

15. S.A. Orszag, "Accurate Solution of the Orr-Sommerfeld Equation." J. Fluid Mech. 50, 689(1971).

16. R.F. Blackwelder and R.E. Kaplan, "Intermittent Structures in Turbulent Boundary Layers." Turbulent Shear Flows, AGARD Conf. Proc. No. 93 (1972).

1. Report No.	2. Government Accession No.	3. Recipient's Catalog No.
NASA CR-2911		

4. Title and Subtitle	5. Report Date
PREDICTION OF COMPLIANT WALL DRAG REDUCTION - PART I	November 1977
	6. Performing Organization Code

7. Author(s)	8. Performing Organization Report No.
Steven A. Orszag	
	10. Work Unit No.

9. Performing Organization Name and Address	11. Contract or Grant No.
Cambridge Hydrodynamics Incorporated P. O. Box 249 M.I.T. Station Cambridge, MA 02139	NAS1-14275

12. Sponsoring Agency Name and Address	13. Type of Report and Period Covered
National Aeronautics and Space Administration Washington, DC 20546	Contractor Report
	14. Sponsoring Agency Code

15. Supplementary Notes

Langley Technical Monitor: Jerry N. Hefner
Final Report

16. Abstract

Computer codes developed to test Bushnell's compliant wall drag reduction model are discussed. One code computes the evolution of mean velocity profiles during the period between bursts as forced by an imposed large-scale pressure pulse due to earlier bursts. Another code computes the local stability characteristics of these computed profiles. The programs use Chebyshev polynomials to resolve the normal boundary layer (y) direction and a staggered grid of mesh points to resolve the x direction. Typically, 257 grid points and 33 Chebyshev polynomials are used in the computations.

17. Key Words (Suggested by Author(s))	18. Distribution Statement
Compliant walls Viscous drag reduction Computational fluid dynamics	Unclassified - Unlimited Subject Category 34

19. Security Classif. (of this report)	20. Security Classif. (of this page)	21. No. of Pages	22. Price*
Unclassified	Unclassified	40	$4.00

* For sale by the National Technical Information Service, Springfield, Virginia 22161

NASA-Langley, 1977